RSC Advances

ROYAL SOCIETY OF CHEMISTRY

www.rsc.org/advances

Graphic Abstract

Functionalization of biodegradable hyperbranched poly(α,β-malic acid) as nanocarrier platform for anticancer drug delivery

Ting Su, Xinyu Peng, Jun Cao, Jing Chang, Rong Liu, Bin He* and Zhongwei Gu

A facile strategy for fabricating hyperbranched poly(α,β-malic acid) nanoparticles with multiple functions was developed for anticancer drug delivery.

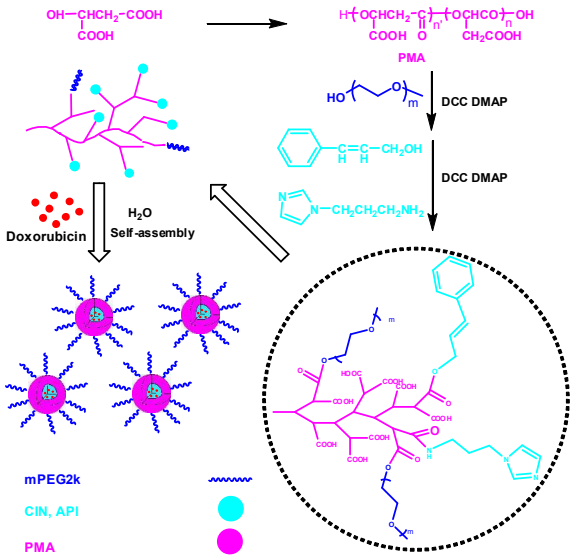

Cite this: DOI: 10.1039/c0xx00000x

www.rsc.org/xxxxxx

ARTICLE TYPE

Functionalization of biodegradable hyperbranchedpoly(α,β-malic acid) as nanocarrier platform for anticancer drug delivery

Ting Su,[a] Xinyu Peng,[a] Jun Cao,[a] Jing Chang,[b] Rong Liu,[c] Zhongwei Gu[a] and Bin He*[a]

Received (in XXX, XXX) Xth XXXXXXXXX 20XX, Accepted Xth XXXXXXXXX 20XX
DOI: 10.1039/b000000x

Multiple functionalization of nanoparticles has attracted great interest in drug delivery. In this paper, biodegradable poly(α,β-malic acid) with hyperbranched architecture was synthesized via the polycondensation of L-malic acid, the functionalized poly(α,β-malic acid) was used as a nanocarrier platform with the immobilization of poly(ethylene glycol) (PEG) for long circulation, cinnamyl alcohol (CIN) for introducing π-π stacking interaction and 1-(3-aminopropyl) imidazole (API) for pH-sensitivity. The conjugates self-assembled into nanoparticles to load anticancer drug doxorubicin (DOX). The morphology, mean size and size distribution, drug release profile and in vitro anticancer activity of DOX loaded nanoparticles were studied. The results showed that the mean size of the nanoparticles was below 200 nm, the drug loading content was higher than 10 wt% and it increased with increasing CIN content because of the π-π stacking interaction between DOX and carriers. The drug release of the nanoparticles was faster in the medium with pH 6.0 comparing to pH 7.4. The nanoparticles exhibited endosomal escape function to accelerate the release of DOX in cancer cells, which resulted in low IC_{50}s to kill 4T1 breast cancer cells and HepG2 liver cancer cells in vitro.

Introduction

In the past two decades, nanoparticles self-assembled from polymeric amphiphiles have been extensively studied for drug delivery.[1-4] Self-assembly is a simple protocol to load hydrophobic anticancer drugs in nanoparticles,[5-7] which is an attractive strategy for fabricating nanomedicine and exhibits great potential clinic applications as a paclitaxel loaded poly(lactic acid)-poly (ethylene glycol) (PLA-PEG) nanoparticle (Genexol-PM) has been approved by FDA for clinic trial.[8] High drug loading content and long circulation are two important aspects in nanomedicine. PEG conjugation is well known to achieve long circulation in drug delivery.[9, 10] High drug loading content is still a problem to be resolved in polymeric nanoparticles.[11, 12] Introduction of interactions such as host-guestinteraction,[13] electrostatic interaction[14] and hydrogen bonding[15] between drugs and nanoparticles was reported to enhance drug loading content, however, there were specificities to design the architectures of nanoparticles and drugs. As most hydrophobic anticancer drugs have π-π conjugated moieties, we have evoked π-π stacking interaction between drugs and carriers to improve the drug loading content.[16, 17]

Intelligent drug delivery are expected to release drugs in a controllable manner upon arrival at the target site in response to external or internal stimuli.[14, 18] pH-dependent drug release is one of the most successful strategies in tumor drug delivery systems.[19-21] Taking the advantages of the weak acidic microenvironment of tumor tissues,[22] many pH-sensitive nanoparticles were fabricated to improve therapeutic efficacy and reduce side effects.[23-25] Poly(L-histidine) based nanoparticles exhibited excellent pH-sensitivity due to the protonation of side imidazole groups in weak acidic medium,[26, 27] however, the complicated synthesis and low yield of poly(L-histidine) limited its wide applications. With the inspiration of pH-sensitivity originated from the protonation of imidazole groups in poly(L-histidine), other nanoparticles with imidazole groups as pH-sensitive moieties were achieved.[28-32]

Poly (malic acid) (PMA) is a water-soluble, biodegradable, and bioabsorbable polymer,[33, 34] the degradation product malic acid is an intermediate product in tricarboxyl acid cycle in the metabolism of carbohydrates, which is non-toxic to cells and tissues. Poly(malic acid) has been reported as hydrogel,[35] cell scaffold[36] and drug carriers.[37, 38] The remarkable advantage of poly(malic acid) for biomedical applications is the large number of carboxyl groups on the backbones, which could be used for multiple functionalization. The synthesis of poly(malic acid) was focused on poly(β-malic acid) via ring-opening polymerization of malolactonate.[39, 40] The polycondensation of L-malic acid to receive poly(α,β-malic acid) was rarely reported. Different from the linear architecture of poly(β-malic acid), the polycondensation generated poly(α,β-malic acid) with hyperbranched architecture, the carboxyl groups were in the peripheral sites, which were more convenient and efficient for modification.

The goal of this study was to fabricate poly(α,β-malic acid) based nanoparticles for anticancer drug delivery. Poly(α,β-malic acid) was used as backbone to provide carboxyl groups for the immobilization of hydrophilic poly(ethylene glycol), hydrophobic cinnamyl alcohol and pH-sensitive 1-(3-aminopropyl) imidazole. The functionalized conjugates self-assembled into nanoparticles to trap anticancer drug doxorubicin. The nanoparticle was expected to own the integrated functions of long circulation, high drug loading content and pH-sensitive drug release.

Materials and method

Materials

Methylated poly(ethylene glycol)(M_w=2000 g·mol^{-1}) (mPEG2k), N,N-dicyclohexylcarbodiimide (DCC) and 4-dimethyl aminopyridine (DMAP) were purchased from Sigma-Aldrich Co. (Steinheim, Germany) and used as received. Doxorubicin hydrochloride (DOX·HCl, Shanghai Yingxuan Chempharm Co.Ltd., China) was dissolved in water, the pH value was adjusted to 9.6 to receive doxorubicin.[41] 1-(3-Aminopropyl) imidazole (API) and cinnamyl alcohol (CIN) was purchased from TCI (Japan). L-malic acid was purchased from Aladdin (China). Dulbecco's Modified Eagle's Medium (DMEM), Roswell Park Memorial Institute (RPMI) 1640 medium, fetal bovine serum (FBS), 4',6-diamidino-2-phenylindole (DAPI) and LysoTracker green (Invitrogen, USA) were used for cells test. Tetrahydrofuran (THF) and diethyl ether were purified before use. All the other solvents were purchased from Kelong Chemical Co. (Chengdu, China) and used without further purification.

Characterizations

^{1}H NMR spectra and Fourier transform infrared (FTIR) spectra were employed to identify the chemical structure of the synthetic polymers. ^{1}H NMR spectra were recorded on a Bruker 400 MHz spectrometer. Samples were dissolved in D_2O or $CDCl_3$ with tetramethylsilane as the internal standard. FTIR spectra were recorded on a Thermo Scientific Nicolet iS10 spectrophotometer over the wavenumber range of 4000-400 cm^{-1}. Gel permeation chromatography (GPC) measurement was carried out on a Waters instrument equipped with a model 1515 pump, a 2414 refractive index detector, and a Waters model 717 auto sampler, the eluent was water and the flow rate was 1 mL/min at 25 °C.

Synthesis of poly(α,β-malic acid) (PMA)

50 g of L-malic acid was added to a 250 mL bottom-round flask with a magnetic stirrer. The polycondensation was carried out at 110 °C under 0.1 mm Hg vacuum for 72 h. The product was dissolved in anhydrous THF and precipitated in large amount of anhydrous diethyl ether. After the diethyl ether was removed, the white precipitate was vacuum-dried at room temperature for 48 h.

Synthesis of PMA-g-mPEG

6.90 g of mPEG2k and 4 g of PMA were dissolved in 150 mL of anhydrous THF in an ice bath under nitrogen atmosphere. A solution of DCC (1.42 g, 6.90 mmol) and DMAP (0.0420 g, 0.345 mmol) in THF (50 mL) was added dropwise into the mixture. The mixture was stirred atroom temperature for 48 h. The white solid dicyclohexylurea (DCU) precipitate was filtrated. The filtrate was condensed and precipitated in large amount of diethyl ether. This procedure was repeated for three times. The white powder was vacuum-dried at room temperature for 48 h.

Synthesis of PMA-g-mPEG-g-CIN/API

Four conjugates with different molar ratio of CIN and API were synthesized (Table 1). Prescribed amounts of CIN, API and PMA-g-mPEG were dissolved in 100 mL of anhydrous THF in an ice bath under nitrogen atmosphere. DCC (the mole ratio of DCC to the total of CIN and API was 2:1) and DMAP (the mole ratio of DMAP to total CIN and API was 0.1:1) were dissolved in anhydrous THF and added to the mixture dropwise. The mixture was magnetically stirred at 0 °C for 48 h. White precipitate appeared in the mixture and the mixture was filtrated. The filtrate was condensed and precipitated in large amount of diethyl ether. This process was repeated for 3 times. The white powder was vacuum-dried at room temperature for 48 h.

Buffering capacity measurement

The buffering capacity of the polymers was examined using the acid-base titration method. Briefly, 2 mL of polymer solution was adjusted initially to pH 10 by 0.1 M NaOH. Then, the polymer solutions were titrated to pH 4.0 with aliquots of 10 μL of 0.1 M HCl. The pH value of the solutions were checked after each addition with a pH-meter (model F-52T, Horiba, Kyoto, Japan).

Preparation of drug loaded nanoparticles

The amphiphilic conjugates (PMA-g-mPEG-g-CIN/API, 20 mg) and DOX (5 mg) were dissolved in 1 mL of DMSO. The solution was stirred at room temperature for 3 h before dropped into 20 mL of deionized water with vigorous stirring. The solution was then transferred to a dialysis tubing (Spectra/PorMWCO=1000) and dialyzed against deionized water at 4 °C for18 h. The outer phase was replaced with fresh deionized water every 4 h till the organic solvent was eliminated. The solution in the tubing was lyophilized after centrifugation (3000 r/min, 5 min). The whole procedure was performed in the dark. The content of encapsulated DOX was determined by UV-Vis measurement (maximum absorption wavelength at 480 nm)with the calibration curve of DOX-DMSO solution. Drug loading content (DLC) and drug loading efficiency (DLE) were calculated according to the following formulas:

$$\text{DLC (wt \%)} = \frac{\text{mass of DOX in the nanoparticles}}{\text{weight of drug-loaded nanoparticle}}\ 100\ \%$$

$$\text{DLE (wt \%)} = \frac{\text{weight of drug in nanoparticle}}{\text{weight of drug in feeding}} \times 100\ \%$$

Size and morphology of nanoparticles

The mean diameter and size distribution of the nanoparticles were determined by dynamic light scattering (DLS, Malvern ZetasizerNano ZS). Each sample was filtered through a 450 nm syringe filter before analysis. Transmission electron microscopy (TEM, JEM-100CX-JEOL) was employed to observe the morphology of the micelles. The TEM samples were prepared by dipping the freshly prepared micelles solution on copper grids and dried at room temperature for few hours before observation.

Interaction between DOX and nanoparticles

UV-Vis absorption and fluorescence spectra were used to exam the π-π interaction in the drug-loaded nanoparticles. The absorbance of DOX loaded nanoparticles was recorded on a Lambda 650S UV-Vis spectrometer (Perkin-Elmer) in the range of 500 to 700 nm. The fluorescence intensity of DOX was determined by fluorescence spectroscopy(F-7000, HITACHI, Japan) at an emission wavelength of 560 nm and an excitation wavelength of 480 nm.

Drug release profile

The lyophilized DOX loaded nanoparticles were dispersed in 1 mL of buffer solution with different pH values (pH 7.4 and 6.0,

ionic strength = 0.01 M). The solutions were transferred in dialysis tubings (Spectra/Por MWCO=1000). The tubings were immersed in vials containing 25 mL of buffer solution with different pH values. The vials were put in a shaking bed at 37 °C with the shaking rate of 150 rpm. 1 mL of medium with released drug was taken out at predetermined time intervals for fluorescence measurement and the same volumes of fresh media were added into the vials. The released DOX was detected by a fluorescence detector with an excitation wavelength at 480 nm and emission wavelength at 550 nm. The release experiments were conducted in triplicate under sink conditions, the mean value was presented.

Cytotoxicity assessment

Mice breastcancer cells 4T1 were cultured in RPMI 1640 media, HepG2 and C2C12 cells were cultured in DMEM medium supplemented with 10% fetal bovine serum (FBS) and 1% penicillin-streptomycin. The cells were cultured at 37 °C in a humidified atmosphere with 5% CO_2. The cells were harvested with 0.02% EDTA and 0.025% trypsin and rinsed. The resulting cell suspension was used in the following experiments.

The cytotoxicity of blank nanoparticles was tested by Cell Counting Kit-8 assay(CCK-8,Dojindo, Japan) against 4T1 breast cancer cells, HepG2 liver cancer cells and C2C12 cells. 4T1 and C2C12 cells were seeded in 96-well plates with the cell density of 4×10^3 mL^{-1}, HepG2 cells were seeded in 96-well plates with a cell density of 6×10^3 mL^{-1}. Each well was cultured with 100 μL of medium. After 24 h incubation, the culture medium was removed and replaced with 100 μL of medium containing blank nanoparticles. The cells were incubated for another 48 h. The culture medium was removed and the wells were rinsed with PBS (pH = 7.4). 100 μL of CCK-8 (volume fraction 10%) solution was added to each well. After incubated for 2 h, the absorbance was measured at a Thermo Scientific MK3 (Thermo fisher, US) at the wavelength of 450 nm.

Cellular uptake

Confocal laser scanning microscopy (CLSM) was employed to examine the cellular uptake of DOX loaded nanoparticles. 4T1 and HepG2 cells at a logarithm phase were seeded on glass dishes (diameter=35 mm) at a cell density of 1×10^4 mL^{-1}. After incubating for 24 h, DOX loaded nanoparticles were dissolved in each culture medium until the final DOX concentration was 10 $\mu g\cdot mL^{-1}$, the culture medium was removed and 200 μL of the mixture was added into each dish. After incubated for 1 and 4 h, the culture medium was removed and the dishes were rinsed with PBS (pH = 7.4).The cell nuclei were stained with DAPI and the culture medium was replaced with PBS. DOX was excited at 480 nm with emission at 590 nm.

In order to explore the effect of API functionalized DOX loaded nanoparticles on endosomal escape for efficient intracellular trafficking, LysoTracker green was used to observe the cytoplasmic distribution of DOX loaded nanoparticles. 4T1 cells at a logarithm phase were seeded on glass dishes (diameter=35 mm) at a cell density of 1×10^4 mL^{-1}. After incubated for 24 h, DOX loaded nanoparticles were dissolved in RPMI 1640 medium till the final DOX concentration was 10 $\mu g\cdot mL^{-1}$, the culture medium was removed and 200 μL of the mixture was added into each dish. After incubated for 1 and 4 h, the culture medium was removed and the dishes were rinsed with PBS (pH = 7.4), and then stained with 50 nM LysoTracker green (Invitrogen, USA) for 60 min at 37 °C. The cells were washed by PBS (pH = 7.4) twice and observed by CLSM.

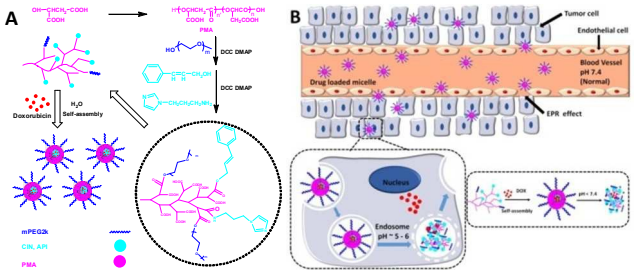

Scheme 1. The synthetic route (A) and the concept for a proposed behavior of polymeric nanoparticles for anticancer drug doxorubicin delivery (B).

For the flowcytometry tests, 4T1 cells were seeded in 6-well plates at a density of 1×10^6 cells per well and incubated for 24 h. The cells were treated with DOX loaded nanoparticles at the same DOX concentration (10$\mu g\cdot mL^{-1}$) for 1 and 4 h, respectively. The culture medium was eliminated, the cells were washed with PBS for three times and harvested by trypsinization. The cells were resuspended in PBS after centrifugation (1000 rpm, 5 min) and the fluorescence intensity was measured (excitation: 480 nm; emission: 590 nm) on a BD FACS Calibur flow cytometer (Beckton Dickinson).

In vitro anticancer activityc

The anticancer activity of drug loaded nanoparticles was evaluated in vitro with 4T1 and HepG2 cells. Cells were harvested and seeded in 96-well plates at a density of 1×10^4 cells per well with 100 μL medium. After 24 h incubation, the medium was replaced with a fresh culture solution containing DOX loaded nanoparticles with different DOX concentrations and incubated for 48 h. Thereafter, the culture medium was removed and the wells were rinsed with PBS (pH 7.4). 100 μL of CCK-8 (volume fraction 10%) solution was added to each well. After incubated for 2h, the absorbance was measured at a Thermo Scientific MK3 (Thermo fisher, US) at the wavelength of 450 nm.

Results and discussion

The synthetic route of the conjugates and the fabrication of nanoparticles were illustrated in Scheme 1. Four conjugates with the same molar ratio of mPEG2k and different molar ratio of API/CIN acted as hydrophobic moieties were synthesized. CIN was introduced for modulating the hydrophobicity and API with a pK_a of 6.5-7.5 range acted as pH-responsive domains in the copolymers.[42-45] mPEG2k was grafted on the pendant carboxyl groups of PMA with 10% molar ratio. API and CIN were immobilized on PMA backbones. The compositions of the four copolymers were shown in Table 1.

The molecular weight and molecular weight distribution of PMA was tested by GPC. The GPC spectrum of PMA was presented in Figure S1 in the Electronic Supplementary Information (ESI). A main peak was observed at the eluent time

about 12.5 minutes and a weak shoulder peak was at 14.5 minutes in the spectrum, the intensity of the main peak was much stronger than that of shoulder peak. The calculated molecular weight was Mn=3780 and the polydispersity was 1.14. The polydispersity of PMA was much narrower than that of theoretical calculated value in polycondensation, which was due to the hyperbranched architecture of PMA.

Table 1. Characterizations of nanoparticles.

entry	compositions			mean size (nm)[a]		PDI		ζpotential (mv)[a]	
	PEG	CIN	API	blank	with DOX	blank	with DOX	blank	with DOX
P1	10	90	0	9± 1.4	29± 1	0.88	0.24	-25±2	-7.4±0.3
P2	10	80	10	67± 12	94±6	0.17	0.15	-7.7±0.2	9.8±0.2
P3	10	70	20	58± 12	60±12	0.14	0.18	-5.6±0.4	4.3±0.4
P4	10	50	40	92± 11	168±8	0.10	0.10	-4.1± 0.2	15± 0.3

[a] Measured by DLS (C = 1 mg/mL), the average size of the three measurements was recorded. The results were expressed as mean ± SD (n=3)

The ^{1}H NMR spectra of PMA and copolymer P4 were shown in Figure 1. The multi-peaks at δ=3.0-3.2 ppm were assigned to the protons of CH_2 in both α and β type units in poly(α,β-malic acid). The protons signals split into multiple peaks due to the random aggregation of α and β type of L-malic acid units in the main chains and the similar chemical environment.[35] The doublets at δ=5.5 and 5.6 ppm were attributed to the protons of C*H* in poly(α,β-malic acid). The peaks at δ=3.4 and 3.6-3.8 ppm were assigned to the protons of OCH_3 and OCH_2CH_2 in mPEG2k. The graft degree was calculated from the intensity ratio between CH_3 in mPEG2k and C*H* in PMA. 10 % of carboxyl groups were grafted on mPEG2k. The characteristic peaks of CIN were assigned to the protons of C*H*=C*H* and CH_2OCO at δ=6.6, 6.2 and 4.7 ppm, respectively. The protons in the benzene ring (C_6H_5) in CIN were detected at δ=7.2-7.5 ppm. The peaks at δ=6.9-7.1 ppm were attributed to protons of imidazole ring in API, and the other three protons of NCH_2CH$_2$, CH$_2$CH_2CH$_2$ and CH$_2$CH_2NH in API were appeared at δ=3.2, 1.8 and 4.1 ppm, respectively. The calculated compositions of the four amphiphiles from ^{1}H NMR spectra were presented in Table 1, they were nearly in agreement with the compositions in feedings. The ^{1}H NMR spectra of copolymers P1, P2 and P3 were presented in Figure S2 in ESI.

The successful conjugation of each amphiphile was further confirmed by FTIR as shown in Figure 2. It was obvious that the vibrations attributed to CH$_2$ at around 2850 cm^{-1} and ether bond CH$_2$OCH$_2$ at around 1100 cm^{-1} were strengthened greatly after mPEG2k was grafted on PMA, and the vibrations of benzene ring at about 690 and 750 cm^{-1} were clear in the FTIR spectrum of P1. The characteristic peak at 1745 cm^{-1} in PMA, P1, P2, P3 and P4 was the stretching vibration absorbance of C=O in ester bond. A new vibration band at 1645 cm^{-1} appeared in P2, P3 and P4, it was the stretching vibration absorbance of C=O in amide bond. At the same time, the peak at 1645 cm^{-1} in the amide bond became stronger comparing to the peak at 1745 cm^{-1} in ester bond with increasing the ratio of API from P2 to P4, suggesting that more API molecules were successfully immobilized on PMA backbones.[31]

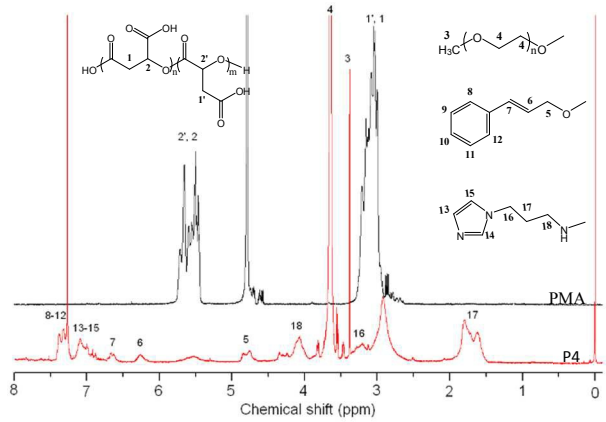

Figure 1. The ^{1}H NMR spectra of PMA and P4 with D_2O (for PMA) and $CDCl_3$ (for P4) as solvents.

The conjugates self-assembled into nanoparticles in aqueous solution. The size distribution and morphology of the nanoparticles were tested by DLS and TEM. The mean diameters and zeta potentials of blank and DOX loaded nanoparticles were summarized in Table 1. All the four conjugates self-assembled into monodisperse nanoparticles (Figure 3A) and the mean size of P1, P2, P3 and P4 were 9, 67, 58 and 92 nanometers. It was interesting that the mean size of P1 was much smaller than that of the other three nanoparticles, the PDI of P1 was the largest. However, when DOX was loaded in the nanoparticles, the mean sizes of all the four nanoparticles were enlarged. The zeta potentials of the four blank nanoparticles increased with increasing the API compositions. The zeta potential of DOX loaded nanoparticles was higher than that of corresponding blank nanoparticles because of the amino group in DOX. The drug loaded nanoparticles were also monodisperse (Figure 3B). The mean size of the drug loaded nanoparticles was smaller than 200 nanometers, which was in suitable size for passive targeting via EPR effect.[46] The morphologies of the blank and DOX loaded nanoparticles were observed by TEM (Figure 3C and 3D), the nanoparticles were well dispersed and the size was consistent with DLS results.[47]

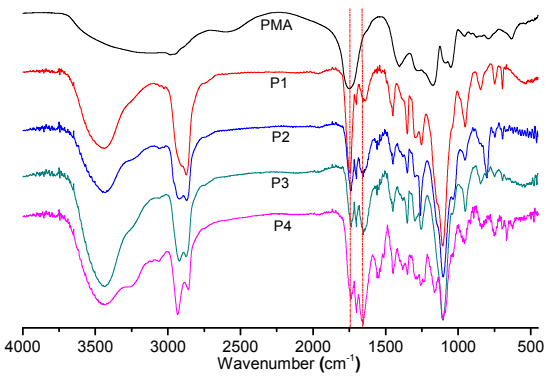

Figure 2. FTIR spectra of PMA, P1, P2, P3 and P4.

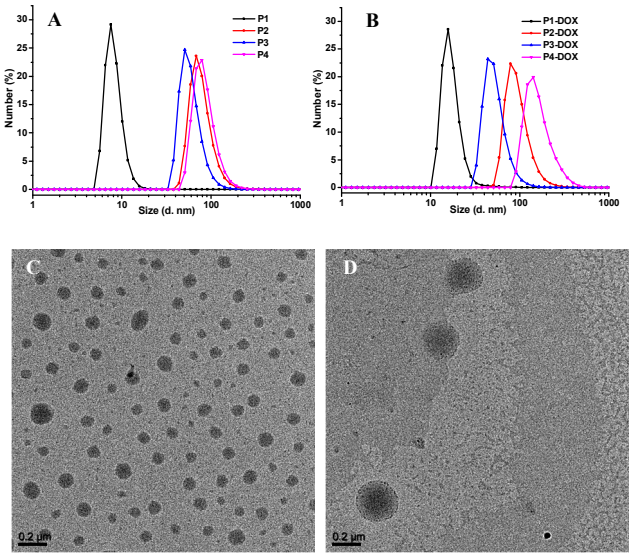

Figure 3. DLS results of blank (A) and DOX loaded nanoparticles (B), TEM images of P4 bank nanoparticles (C) and DOX loaded nanoparticles (D).

The drug loading content (DLC) and drug encapsulation efficiency (DEE) of the four nanoparticles were measured and the results were summarized in Table 2. P1-DOX nanoparticles exhibited the best DLC and DEE. The DLC and DEE of P1-DOX nanoparticles were 15 and 70.6 wt%, respectively, which were much higher than those of the other three nanoparticles. Both DLC and DEE of nanoparticles decreased when the API in the nanoparticles increased, it was probably attributed to the interaction between DOX and nanoparticles.

In our previous work, we reported that the formation of π-π stacking interaction was helpful to enhance the DLC of nanoparticles.[16, 17] In order to verify the π-π interaction and explain the DLC variation in the four nanoparticles, the π-π interaction between nanoparticles and DOX was investigated. The UV-Vis absorption and fluorescence spectra of DOX loaded nanoparticles were tested. The maximum UV absorbance (λ_{max}) of free DOX·HCl was at 483 nm and the blank nanoparticle showed no evident absorption in the wavelength from 350 to 650 nm(Figure 4A). After DOX was encapsulated into the nanoparticles, the absorbance λ_{max} showed a red shift to 497, 498, 498 and 500 nm for P1-DOX, P2-DOX, P3-DOX and P4-DOX, respectively. It implied that π-π stacking interaction within the drug loaded nanoparticles was evoked.[48] The π-π stacking interaction was further investigated via fluorescence measurement as showed in Figure 4B. When the exciting wavelength was set at 483 nm, free DOX performed wide band from 600 to 700 nm. However, DOX loaded nanoparticles exhibited remarkable decrease in the fluorescence intensity of emission band comparing to free DOX at the same concentration. The significant intensity decrease indicated the quenching of fluorescence by energy transfer among π-π interaction overlapped systems.[49] The higher quenching degree of DOX loaded nanoparticles likely demonstrated the stronger π-π interaction. It revealed that the π-π stacking interaction between nanoparticles and DOX was weakened with the composition increase of API in the nanoparticles. That was the intrinsic nature in nanoparticles to affect the drug loading content.

Table 2. Drug loading content and encapsulation efficiency of nanoparticles.

Sample	DLC (wt %)	DEE (wt %)	IC_{50} (μg/mL) [a]	
			4T1	HepG2
P1-DOX	15	70.6	7.89	3.27
P2-DOX	12	54.6	7.61	2.58
P3-DOX	10	44.4	4.53	1.95
P4-DOX	10	44.4	4.78	1.43

[a] The half maximal inhibitory concentration values.

As we knew that the high buffering capacity enable nanoparticles to facilitate endosomal escape,[50, 51] which contributed to efficient drug release. The presence of imidazole units in PMA based nanoparticles was expected to achieve pH-responsive drug release via the protonation of imidazole groups in endosomes. Acid-base titration of the copolymers was carried out to exhibit the buffering capacity of the four conjugates (Figure 5A). The results showed that all copolymers had a buffer platform, indicating all of them exhibited buffering capacity. With the graft degree of API increased, the P4 had the widest buffer platform comparing to the other three, it revealed that the P4 conjugate had better capacity for proton acceptance.

As the pH value in endosomes was about 6.0 and the nanoparticles were encapsulated in endosomes once they were internalized in cells. The drug release profiles of DOX loaded nanoparticles were tested in PBS solutions with pH=7.4 and 6.0 (ionic strength = 0.01 M) at 37 °C (Figure 5B). The amounts of released DOX at different predetermined time points were measured by fluorescence detector with excitation wavelength at 480 nm and emission wavelength at 550 nm. The release performed an early weak burst release in the first few hours and a sustained release in the followed stage for prolonged time. The four drug loaded nanoparticles practically showed no difference in DOX release in the medium with pH 7.4. The cumulated release was less than 20% even the release time was as long as 48 h. However, in the medium with pH=6.0, the drug was released faster from nanoparticles, P4-DOX nanoparticles showed the fastest release within all the four nanoparticles, and the release rates of P2-DOX and P3-DOX nanoparticles showed nearly the same release rates. All the three nanoparticles with API in P2, P3 and P4 exhibited fast DOX release comparing to P1 without API. The release profiles revealed the pH-sensitivity of API.

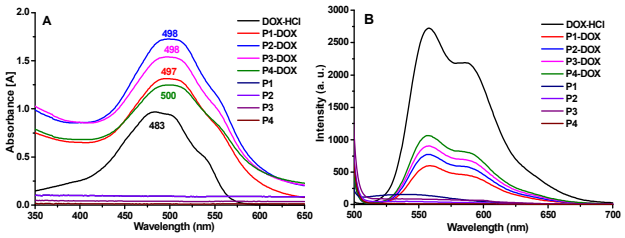

Figure 4. The UV-Vis absorption (A) and fluorescence spectra (B) of blank and DOXloaded nanoparticles, the excitation wavelength of fluorescence spectra was fixed at 480 nm and the DOX concentration was 10 μg/mL.

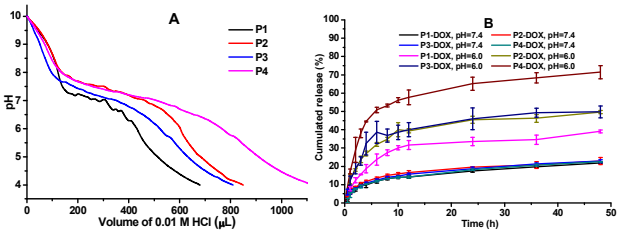

Figure 5. Acid-base titration curves of blank nanoparticles (A) and the release profiles of DOX loaded nanoparticles (B), means ±SD (n = 3).

The cytotoxicity of the polymeric nanoparticles was investigated via CCK-8 assay. The blank nanoparticles were incubated with 4T1 breast cancer cells, C2C12 cells and HepG2 liver cancer cells for 48 h with different concentrations. Figure 6 showed that all the cell viabilities were higher than 90% after incubated with blank nanoparticle for 48 h even the concentration of nanoparticles was as high as 600 μg/mL. It revealed that the four blank nanoparticles were nontoxic to cells.[52]

The delivery efficiency and intracellular localization of DOX loaded nanoparticles in 4T1 cells were investigated using confocal laser scanning microscopy (CLSM). In Figure 7, red fluorescence of DOX was observed cytoplasm in both 4T1 and HepG2 cells in 1 h, which implied that most of the drug loaded nanoparticles were in cytoplasm. The cells treated with P4-DOX nanoparticles exhibited stronger red fluorescence for 1 h incubation, which demonstrated that more P4-DOX nanoparticles were internalized into the cells. The cells showed stronger red fluorescence for 4 h incubation compared with 1 h incubation, it implied that more drug loaded nanoparticles were internalized into cells and a sustained release of DOX from the DOX loaded nanoparticles was happened. The DOX in nanoparticles was more easily diffused in nuclei of HepG2 cells.

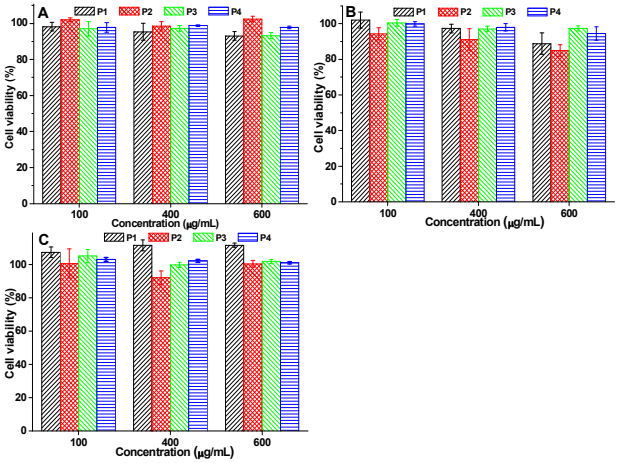

Figure 6. The cytotoxicity of blank nanoparticles incubated with 4T1 cells (A), C2C12 cells (B) and HepG2 cells (C) for 48 h.

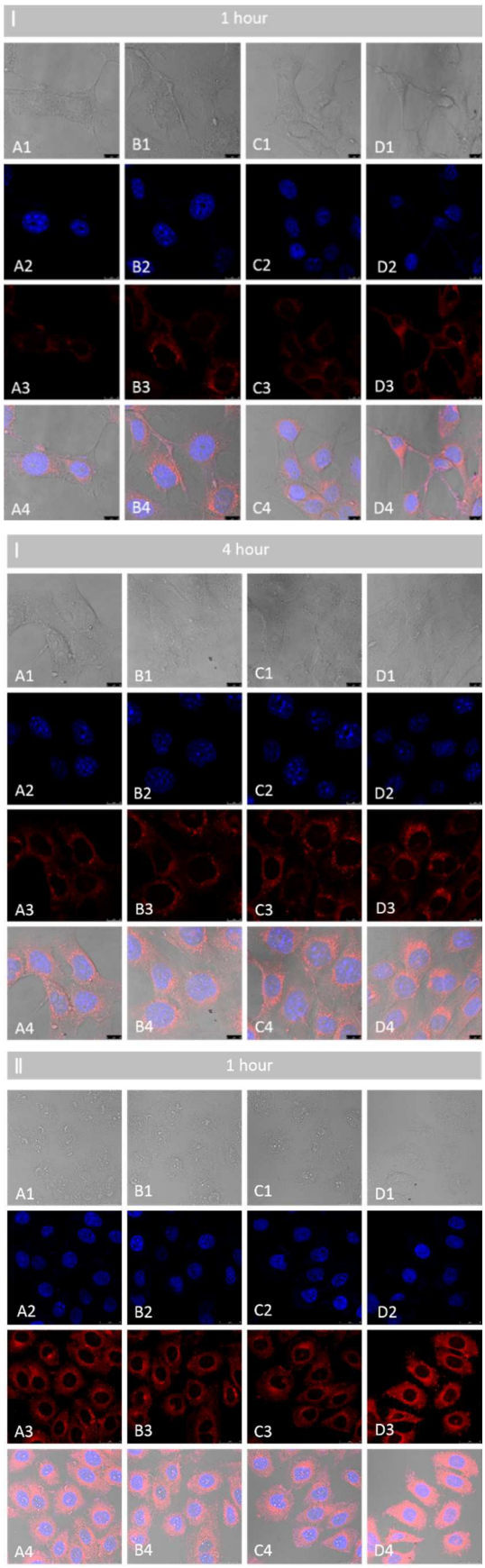

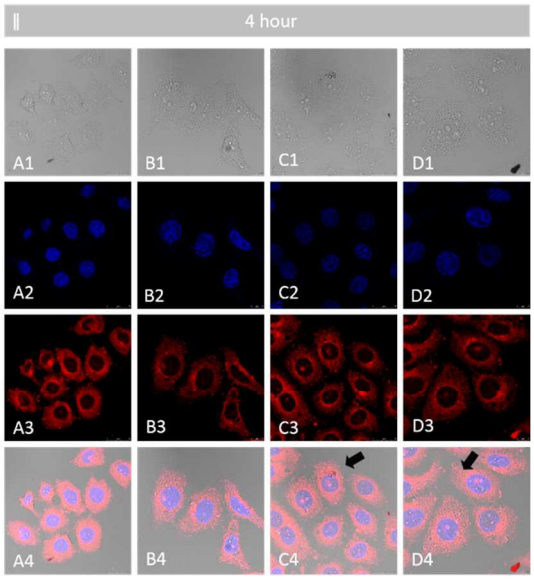

Figure 7. The confocal laser scanning microscopy images of 4T1 cells (I) and HepG2 cells (II) treated with DOX loaded nanoparticles P1-DOX (A), P2-DOX (B), P3-DOX (C), and P4-DOX (D) at 37 °C for 1 h and 4 h. For each panel, the images from top to bottom were cells in bright field (1), DOX fluorescence in cells (2), cell nuclei stained by DAPI (3), and overlay images (4). The DOX concentration was 10 μg/mL and the bar was 25 mm.

To identify the role of imidazole group in pH-responsive nanoparticles of P2, P3 and P4, the intracellular tracking of DOX loaded nanoparticles were studied via CLSM. Lysosomes in 4T1 cells were observed in green fluorescence after they were stained with specific LysoTracker green. DOX loaded nanoparticles were shown in red fluorescence. Co-localization of the DOX loaded nanoparticles overlapped with green-dyed lysosomes appeared yellow. As shown in Figure 8, in the first hour, the red fluorescence was highly overlaid with the green fluorescence and all the four nanoparticles showed yellow fluorescence in the overlay images. Obviously, there was no difference among the four nanoparticles, illustrating that all the DOX loaded nanoparticles were located in lysosomes. In the 4 h images, the P1-DOX nanoparticles showed yellow, demonstrating that it was hard for P1-DOX nanoparticles to escape from endolysosomes.[53, 54] In contrast, although the P2-DOX, P3-DOX and P4-DOX nanoparticles were located in the endolysosomes for the first hour in yellow in the overlay images, however, the green fluorescence had a significant decline and the red fluorescence became stronger, rare yellow fluorescence was observed in the overlay of the images of P2-DOX, P3-DOX and P4-DOX nanoparticles. It clearly indicated that the efficient endolysosomal escape was happened in the imidazole modified DOX loaded nanoparticles (P2-DOX, P3-DOX and P4-DOX). These results revealed the pH-sensitive drug release from API modified PMA based nanoparticles.

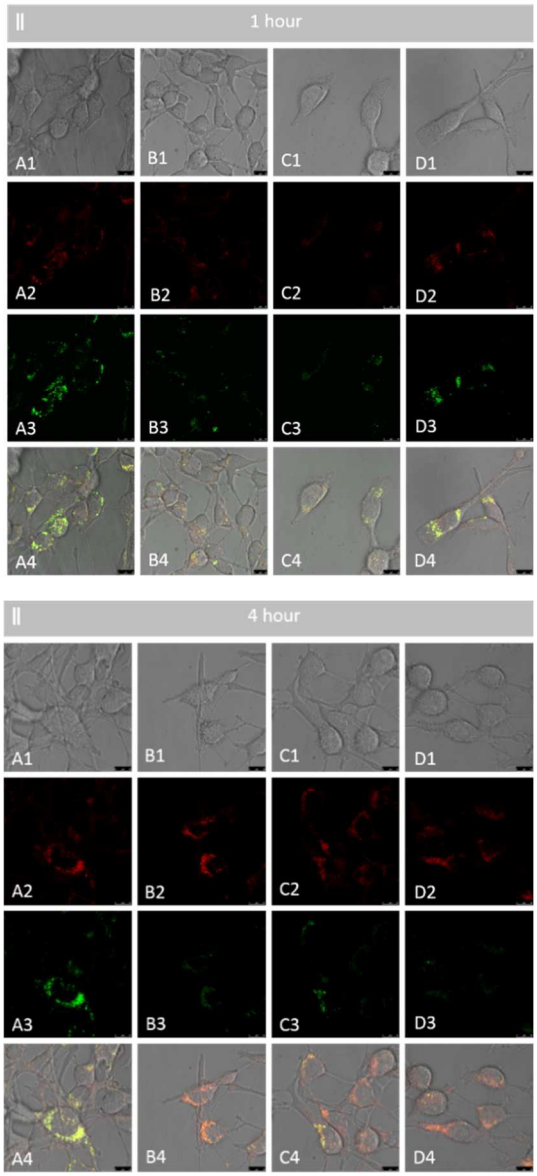

Figure 8. The confocal laser scanning microscopy images of 4T1 cells treated with DOX loaded nanoparticles P1-DOX (A), P2-DOX (B), P3-DOX (C), and P4-DOX (D) at 37 °C for 1 h and 4 h. For each panel, the images from top to bottom were cells in bright field (1), DOX fluorescence in cells (2), lysosomes stained by LysoTracker green (3), and overlay images (4). The DOX concentration was 10 μg/mL and the bar was 25 mm.

The cellular internalization of drug loaded nanoparticles was further illustrated in flow cytometry. The intracellular delivery efficiency of DOX loaded nanoparticles in 4T1 cells was given in quantitative fluorescence intensity. Figure 9A and 9B showed the results of 4T1 breast cancer cells treated with DOX loaded nanoparticles for 1 (Figure 9A) and 4 h (Figure 9B), respectively. The concentration of DOX was the same as 10 μg/mL. The mean red fluorescence intensities of 4T1 cells for different incubation times were presented in Figure 9C. The cells incubated with P4-DOX nanoparticles showed the highest red fluorescence intensity. There was no significant difference in the mean fluorescence intensity among the four nanoparticles for 1 h incubation as

shown in the quantitative results in Figure 9C. When the incubation time was extended to 4 h, all the nanoparticles showed a stronger red fluorescence in the cells, and the API modified nanoparticles (P2-DOX, P3-DOX and P4-DOX) exhibited higher mean fluorescence intensity comparing to P1-DOX nanoparticles. However, the strongest fluorescencewas observed in P4-DOX nanoparticles. It also revealed the pH-sensitivity of API modified nanoparticles.

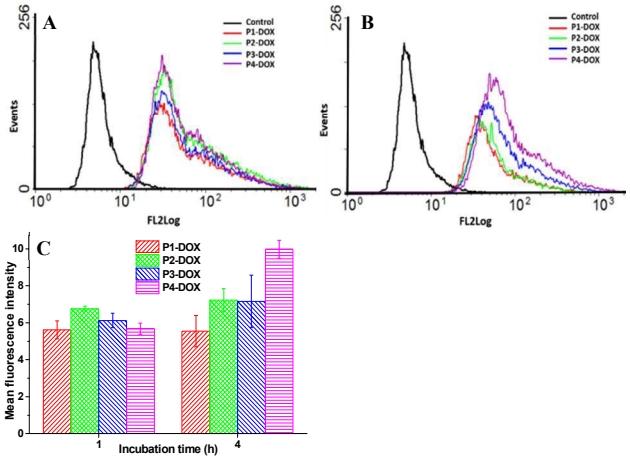

Figure 9. The flow cytometry results of 4T1 cells treated with DOX loaded nanoparticles for 1 h (A) and 4 h (B). The mean fluorescence intensity (FL2) of 4T1 cells treated with the DOX loaded nanoparticles for 1 and 4 h (C), the concentration of DOX was 10 μg/mL.

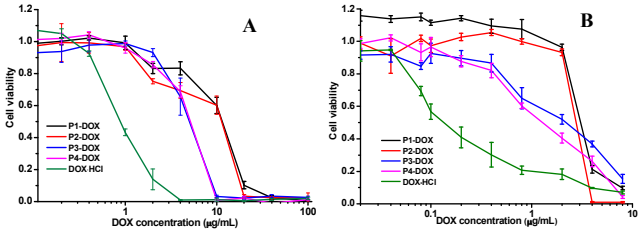

Figure 10. The IC_{50} of the DOX loaded nanoparticles incubated with 4T1 breast cancer cells (A) and HepG2 liver cancer cells (B).

The in vitro anticancer activity of the four DOX loaded nanoparticles was evaluated in 4T1 breast cancer cells and HepG2 liver cancer cells via CCK-8 assay. As shown in Figure 10, the IC_{50}s (half maximal inhibitory concentration) values of the four DOX loaded nanoparticles of 4T1 cells for P1-DOX, P2-DOX, P3-DOX, P4-DOX and DOX·HCl were 7.89, 7.61, 4.53, 4.78 and 0.79 μg/mL, and the IC_{50}s for HepG2 cells were 3.27, 2.58, 1.95, 1.43 and 0.17 μg/mL as shown in Table 2. Once the drug loaded nanoparticles were internalized into cytoplasm via endocytosis, the protonation of imidazole groups began to take effect in the weak acidic environment of endosomes, and the resulting proton sponge effect accelerated the release of DOX.[53] The imidazole group in API was beneficial to help drug loaded nanoparticles to escape from endosomes and release DOX to facilitate the diffusion into nucleus to inhibit the proliferation of cells. P3-DOX and P4-DOX nanoparticles showed the lower IC_{50}s with more efficient in vitro anticancer activity due to the higher composition of API in the nanoparticles. DOX·HCl was a water-soluble molecule, which diffused much faster into cells to kill cells efficiently and resulted in lowest IC_{50}s.

Conclusions

In summary, we successfully developed a functionalized poly(α,β-malic acid) based nanocarrier platform for anticancer drug delivery.mPEG, cinnamyl alcohol and 1-(3-aminopropyl) imidazole were immobilized on the carboxyl groups of poly(α,β-malic acid). The conjugates self-assembled into nanoparticles to load anticancer drug doxorubicin with the functions of long circulation, pH-sensitivity and π-π stacking interaction. The mean size of the drug loaded nanoparticles was smaller than 200 nanometers and well dispersed in aqueous medium. The π-π stacking interaction between drug and nanoparticle was helpful to improve the drug loading, the drug loading content was higher than 10 wt%. The protonation of imidazole groups in the nanoparticles facilitated the endosomalescapeof the loaded drug and promoted the anticancer activity. These findings demonstrated the feasibility of pH sensitive nanomedicine for effective chemotherapy.

Acknowledgement

This research work was supported by National Science Foundation of China (No. 51222304, 31170921,51403137, 31100676, 51203157), Doctoral Fund of Ministry of Education of China (No. 20130181110038), Young teachers' scientific research foundation of Sichuan University (2014SCU11015).

Notes and references

[a]*National Engineering Research Center for Biomaterials, Sichuan University, Chengdu 610064 China. Fax: +86-28-85412923; Tel: +86-28-85412923; E-mail: bhe@scu.edu.cn*
[b]*College of Marine Life Science, Ocean University of China, Qingdao 266003 China. Fax: +86-532-82032105; Tel: +86-532-82032109; E-mail: jingjing_ch@yahoo.com.cn*
[c]*College of Medical and Nursing,Chengdu University, Chengdu, 610106 China. Fax: +86-86-85616523; Tel: +86-28-85616523; E-mail: liurongscu@126.com*
[*]*Corresponding author.*

† Electronic Supplementary Information (ESI) available: [details of any supplementary information available should be included here]. See DOI: 10.1039/b000000x/

‡ Footnotes should appear here. These might include comments relevant to but not central to the matter under discussion, limited experimental and spectral data, and crystallographic data.

1. W. Zhang, Y. Li, L. Liu, Q. Sun, X. Shuai, W. Zhu and Y. Chen, *Biomacromolecules*, 2010, 11, 1331-1338.
2. J. Liu, W. Huang, Y. Pang, X. Zhu, Y. Zhou and D. Yan, *Langmuir*, 2010, 26, 10585-10592.
3. X. Qian, L. Long, Z. Shi, C. Liu, M. Qiu, J. Sheng, P. Pu, X. Yuan, Y. Ren and C. Kang, *Biomaterials*, 2014, 35, 2322-2335.
4. Q. Liu, H. Zhu, J. Qin, H. Dong and J. Du, *Biomacromolecules*, 2014, 15, 1586-1592.
5. A. Schulz, S. Jaksch, R. Schubel, E. Wegener, Z. Di, Y. Han, A. Meister, J. Kressler, A. V. Kabanov, R. Luxenhofer, C. M. Papadakis and R. Jordan, *ACS Nano*, 2014, 8, 2686-2696.

6. Q. Yin, J. Shen, Z. Zhang, H. Yu, L. Chen, W. Gu and Y. Li, *Biomacromolecules*, 2013, 14, 2242-2252.
7. D. Wang, Y. Su, C. Jin, B. Zhu, Y. Pang, L. Zhu, J. Liu, C. Tu, D. Yan and X. Zhu, *Biomacromolecules*, 2011, 12, 1370-1379.
8. K. Zhang, X. Tang, J. Zhang, W. Lu, X. Lin, Y. Zhang, B. Tian, H. Yang and H. He, *Journal of Controlled Release*, 2014, 183, 77-86.
9. M. J. Joralemon, S. McRae and T. Emrick, *Chemical Communications*, 2010, 46, 1377-1393.
10. S. Sunoqrot, J. Bugno, D. Lantvit, J. E. Burdette and S. Hong, *Journal of Controlled Release*, 2014, 191, 115-122.
11. Y. Sun, W. Zou, S. Bian, Y. Huang, Y. Tan, J. Liang, Y. Fan and X. Zhang, *Biomaterials*, 2013, 34, 6818-6828.
12. Y. Shen, E. Jin, B. Zhang, C. J. Murphy, M. Sui, J. Zhao, J. Wang, J. Tang, M. Fan, E. Van Kirk and W. J. Murdoch, *Journal of the American Chemical Society*, 2010, 132, 4259-4265.
13. L. Wang, L.-l. Li, Y.-s. Fan and H. Wang, *Advanced Materials*, 2013, 25, 3888-3898.
14. J. Ding, C. Xiao, Y. Li, Y. Cheng, N. Wang, C. He, X. Zhuang, X. Zhu and X. Chen, *Journal of Controlled Release*, 2013, 169, 193-203.
15. H. Kuang, S. Wu, F. Meng, Z. Xie, X. Jing and Y. Huang, *Journal of Materials Chemistry*, 2012, 22, 24832-24840.
16. Y. Lai, Y. Lei, X. Xu, Y. Li, B. He and Z. Gu, *Journal of Materials Chemistry B*, 2013, 1, 4289-4296.
17. Y. Li, T. Su, S. Li, Y. Lai, B. He and Z. Gu, *Biomaterials Science*, 2014, 2, 775-783.
18. J. Zhao, H. Wang, J. Liu, L. Deng, J. Liu, A. Dong and J. Zhang, *Biomacromolecules*, 2013, 14, 3973-3984.
19. T. Xing, X. Yang, F. Wang, B. Lai and L. Yan, *Journal of Materials Chemistry*, 2012, 22, 22290-22300.
20. Y. Huang, Z. Tang, X. Zhang, H. Yu, H. Sun, X. Pang and X. Chen, *Biomacromolecules*, 2013, 14, 2023-2032.
21. W. Feng, W. Nie, C. He, X. Zhou, L. Chen, K. Qiu, W. Wang and Z. Yin, *ACS Applied Materials & Interfaces*, 2014, 6, 8447-8460.
22. Z. Ge and S. Liu, *Chemical Society Reviews*, 2013, 42, 7289-7325.
23. F. Shi, J. Ding, C. Xiao, X. Zhuang, C. He, L. Chen and X. Chen, *Journal of Materials Chemistry*, 2012, 22, 14168-14179.
24. S. Zhu, M. Niu, H. O'Mary and Z. Cui, *Molecular Pharmaceutics*, 2013, 10, 3525-3530.
25. Z. Poon, D. Chang, X. Zhao and P. T. Hammond, *ACS Nano*, 2011, 5, 4284-4292.
26. H. Yin, H. C. Kang, K. M. Huh and Y. H. Bae, *Journal of Materials Chemistry*, 2012, 22, 19168-19178.
27. R. Liu, D. Li, B. He, X. Xu, M. Sheng, Y. Lai, G. Wang and Z. Gu, *Journal of Controlled Release*, 2011, 152, 49-56.
28. F. C. Giacomelli, P. Stepanek, C. Giacomelli, V. Schmidt, E. Jager, A. Jager and K. Ulbrich, *Soft Matter*, 2011, 7, 9316-9325.
29. X. Hu, X. Guan, J. Li, Q. Pei, M. Liu, Z. Xie and X. Jing, *Chemical Communications*, 2014, 50, 9188-9191.
30. C. Fang, F. M. Kievit, Y.-C. Cho, H. Mok, O. W. Press and M. Zhang, *Nanoscale*, 2012, 4, 7012-7020.
31. Y. Pu, L. Zhang, H. Zheng, B. He and Z. Gu, *Polymer Chemistry*, 2014, 5, 463-470.
32. C.-S. Lee, W. Park, Y. U. Jo and K. Na, *Chemical Communications*, 2014, 50, 4354-4357.
33. M. Fujita, B.-S. Lee, N. M. Khazenzon, M. L. Penichet, K. A. Wawrowsky, R. Patil, H. Ding, E. Holler, K. L. Black and J. Y. Ljubimova, *Journal of Controlled Release*, 2007, 122, 356-363.
34. H. Ding, G. Helguera, J. A. Rodríguez, J. Markman, R. Luria-Pérez, P. Gangalum, J. Portilla-Arias, S. Inoue, T. R. Daniels-Wells, K. Black, E. Holler, M. L. Penichet and J. Y. Ljubimova, *Journal of Controlled Release*, 2013, 171, 322-329.
35. B. He, E. Wan and M. B. Chan-Park, *Chemistry of Materials*, 2006, 18, 3946-3955.
36. N. Qiang, W. Yang, L. Li, P. Dong, J. Zhu, T. Wang, C. Zeng and D. Quan, *Polymer*, 2012, 53, 4993-5001.
37. J. Wang, C. Ni, Y. Zhang, M. Zhang, W. Li, B. Yao and L. Zhang, *Colloids and Surfaces B: Biointerfaces*, 2014, 115, 275-279.
38. B.-S. Lee, M. Fujita, N. M. Khazenzon, K. A. Wawrowsky, S. Wachsmann-Hogiu, D. L. Farkas, K. L. Black, J. Y. Ljubimova and E. Holler, *Bioconjugate Chemistry*, 2006, 17, 317-326.
39. B. He, Y. Wan, J. Bei and S. Wang, *Biomaterials*, 2004, 25, 5239-5247.
40. B. He and M. B. Chan-Park, *Macromolecules*, 2005, 38, 8227-8234.
41. X. Shuai, H. Ai, N. Nasongkla, S. Kim and J. Gao, *Journal of Controlled Release*, 2004, 98, 415-426.
42. J. Y. Yhee, S. Lee and K. Kim, *Nanoscale*, 2014, DOI: 10.1039/C4NR04334K.
43. E. S. Lee, J. H. Kim, T. Sim, Y. S. Youn, B.-J. Lee, Y. T. Oh and K. T. Oh, *Journal of Materials Chemistry B*, 2014, 2, 1152-1159.
44. D. Ling, W. Park, S.-j. Park, Y. Lu, K. S. Kim, M. J. Hackett, B. H. Kim, H. Yim, Y. S. Jeon, K. Na and T. Hyeon, *Journal of the American Chemical Society*, 2014, 136, 5647-5655.
45. A. Sharma and A. Srivastava, *Polymer Chemistry*, 2013, 4, 5119-5128.
46. K. Raemdonck, K. Braeckmans, J. Demeester and S. C. De Smedt, *Chemical Society Reviews*, 2014, 43, 444-472.
47. H. Arimura, Y. Ohya and T. Ouchi, *Biomacromolecules*, 2005, 6, 720-725.
48. X. Yang, X. Zhang, Z. Liu, Y. Ma, Y. Huang and Y. Chen, *The Journal of Physical Chemistry C*, 2008, 112, 17554-17558.
49. A. Di Crescenzo, D. Velluto, J. A. Hubbell and A. Fontana, *Nanoscale*, 2011, 3, 925-928.
50. R. Shrestha, M. Elsabahy, S. Florez-Malaver, S. Samarajeewa and K. L. Wooley, *Biomaterials*, 2012, 33, 8557-8568.
51. N. Skandrani, A. Barras, D. Legrand, T. Gharbi, H. Boulahdour and R. Boukherroub, *Nanoscale*, 2014, 6, 7379-7390.
52. Z. Su, L. Xing, Y. Chen, Y. Xu, F. Yang, C. Zhang, Q. Ping and Y. Xiao, *Molecular Pharmaceutics*, 2014, 11, 1823-1834.
53. T. Jiang, Z. Zhang, Y. Zhang, H. Lv, J. Zhou, C. Li, L. Hou and Q. Zhang, *Biomaterials*, 2012, 33, 9246-9258.